



Numerical Parametric Study of Fully Encased Composite Columns Subjected to Cyclic Loading

Almoutaz Bellah Alsamawi ^{1*}, Nadir Boumechra ¹, Karim Hamdaoui ¹

¹ EOLE Research Laboratory, Department of Civil Engineering, Faculty of Technology, University of Tlemcen, BP 230, Tlemcen, Algeria.

Received 28 September 2021; Revised 29 November 2021; Accepted 08 December 2021; Published 01 January 2022

Abstract

This paper investigates the cyclic behaviour of steel-concrete encased composite columns. By investigating the cover concrete and the steel-concrete coefficient of friction on the behaviour (strength, ductility, stiffness, and energy dissipation) of composite columns subjected to combined axial load and cyclically increasing lateral load to improve the strength and performance of the composite column. Eight of the columns were designed to study the cover concrete effect, and eleven other columns were designed to study the coefficient of friction effect in the dynamic behaviour to the cyclic load. Additionally, in this study, the finite element models created in ANSYS software were verified and calibrated against previously published experimental results (load-displacement curve, load capacity and failure mode). The numerical results obtained from the finite element model indicate that the ductility and the energy dissipated increased by +11.71 and +18.93% respectively by the increase of the cover concrete until reaching the limit of the cover concrete. Beyond this limit, the ductility and the energy decrease by 27.33 and 24.97% respectively. The results also indicate that the ductility and the energy dissipated increased by 12.62 and 7.82% respectively by the increased coefficient of friction until reach 0.6, after that the energy decreases by 4.47%.

Keywords: Fully Encased Composite Columns; Coefficient of Friction; Cover Concrete; Cyclic Loading; Hysteresis Curves.

1. Introduction

Composite columns have grown more popular in building constructions in recent years, particularly in seismically active areas and to ensure fire safety. This is because they offer the required rigidity to keep the building's lateral drift to an acceptable level while also efficiently resisting wind loads and lateral seismic. The composite columns will be capable of resisting a high load capacity while also providing economic advantages due to their lower cross-section. The addition of structural steel to the centre of a cross-section column increases the column's ductility while also allowing it to resist tensile loads such as reinforced bars or structural steel sections. Because the steel has high tensile strength, ductility and stiffness, and the concrete has low cost and great compression strength, the two materials should work well together. However, research into the cyclic behaviour of concrete-encased columns has been limited, with the focus on experimental testing of composite columns subjected to cyclic lateral loads. Chen et al. [1] conducted on steel-concrete composite column stirrup ratios and embedding depth ratios. By analysing each specimen's hysteresis loops, energy dissipation, ductility, failure patterns and skeleton curve. It was found that increasing the stirrup ratio improves seismic behaviour, that cross-shaped steel composite columns perform better seismically than H-shaped steel composite columns, and that the embedded ratio of steel-concrete composite columns can be as minimal as 2.5. Zhu et al. [2] investigated how steel-reinforced high strength concrete columns (SRHC) responded under cycle loads using

* Corresponding author: mezo.smawi@gmail.com

 <http://dx.doi.org/10.28991/CEJ-2022-08-01-04>



© 2022 by the authors. Licensee C.E.J, Tehran, Iran. This article is an open access article distributed under the terms and conditions of the Creative Commons Attribution (CC-BY) license (<http://creativecommons.org/licenses/by/4.0/>).

structural steel detailing with studs and stirrup arrangement. SRHC with several stirrups could deform and dissipate energy. SRHC columns performed well at early loading, with studs having little effect. After cover spalling, SRHC columns' seismic behaviour is influenced by studs. Columns with studs can dissipate more energy and deform more, reducing column stiffness degradation.

Campian et al. [3] compared the results of composite encased columns made of high strength concrete to those constructed of normal strength concrete. The findings show that high-strength concrete columns are more susceptible to fragile failure than normal-strength concrete columns and that high-strength concrete has a favourable energy absorption capacity. A recent study has focused on the performance of specially designed columns. It was studied by Fang et al. [4] how loading angles, steel ratios, and axial load ratios affected the behaviour of concrete-encased steel cross-shaped columns. The maximum lateral load increases with axial compression ratio, while stiffness decreases and displacement ductility reduces significantly. Loading at 45° provides a better maximum lateral load than loading at 0° . XU et al. [5] investigated the effects of the presence of cross tie, stirrup ratio, shear span ratio and axial compression level. It was found that the unsymmetrical phenomenon affects the hysteresis curve, with the increase of axial load level the ductility decreases. The cross tie reduces the stiffness degradation and strength attenuation and reinforces the bearing capacity. Previous studies on filled steel tube reinforced concrete columns and encased steel-concrete composite columns indicated that both columns had good ductility and energy dissipation and can be used in seismic areas. Han et al. [6] studied the axial load level and cross-sectional type, by investigating the influence of energy dissipation, stiffness, ductility and strength. It was found that, with increasing axial load level, the energy dissipation ability and the ductility of the columns decreases. Also, the rigidity degradation for specimens with a higher axial load level was less significant than that with a lower axial load level. For concrete-filled steel tube reinforced concrete column, Gajalakshmi et al. [7] investigated the diameter thickness ratio of steel tubes as well as two types of in-fills, plain cement concrete and steel fibre reinforced concrete. By testing concrete-filled steel (CFT) columns and steel fibre reinforced concrete in-filled steel tube (SCFT) columns. The test consisted of benchmark tests to measure the hysteresis behaviour under various amplitude cyclic loading. Compared to SCFT columns, CFT columns have less improved ductility, damage index, and energy absorption capability. Further investigation of encased steel-concrete composite columns has been carried out by other researchers.

Qian et al. [8] conducted the interaction between concrete and steel as well as the cumulative damage of concrete. The results indicate that the axial load level affects the distribution of the axial load between the components. Shim et al. [9] investigated composite columns with less than 4% of steel, loading pattern and the amount of transverse reinforcement. Based on test results, design considerations related to the details of transverse reinforcements of composite columns were suggested. Hsu et al. [10] determined member strengths under combined axial load and bi-axial bending, by proposing the interaction coefficients α and β . Ellobody et al. [11] analysed the effect of concrete confinement as well as the inelastic behaviour of concrete, steel, transverse and longitudinal reinforcement bars, and the interface between the steel section and concrete of the concrete-encased steel composite columns. It is observed that the flexural buckling failure mode has a small effect on the composite column strength of the columns with greater slenderness ratios. Taufik et al. [12] determined the fracture patterns, strain, stress, deformation, ductility and capacity of axial load to analyse the failure behaviour of modelling encased composite steel-concrete columns. The results indicated that the compressive collapse columns have a larger flexural capacity and are less ductile than those columns with tensile collapse, while the analysis of calculation and finite element method determined the behaviour of composite columns.

Chen et al. [13] carried out on the rational scope of the width-thickness ratio of encased steel flange, benefiting the post-buckling capacity of steel also the width-thickness ratio, of partially encased composite columns with thin-walled H-shaped steel plates. It was discovered that axial compression load does not exceed encased capacity and the width-thickness ratio does not exceed Eurocode 4 limits, a favourable energy dissipation capacity and ductile failure mode can be predicted. Naito et al. [14] investigated the ductility of concrete-encased steel piers. The ultimate state and the recoverable boundary state were defined as the local buckling of the H-steel and the spalling of the concrete cover, respectively. Yue et al. [15] investigated cover concrete spalling, cover concrete cracking, core concrete crushing, steel flange local buckling, compressive longitudinal reinforcement yielding, and longitudinal reinforcement buckling in concrete-encased steel columns under high axial compressive ratios and low-cyclic lateral loading. It can be observed from the previous works that researches into the behaviour of composite columns are still not yet sufficient to fully understand the behaviour of composite columns under cyclic or seismic loads. It is necessary to focus on the effects of geometrical, physical and mechanical characteristics as the cover concrete, the coefficient of friction, loading and others.

Therefore, nineteen designed specimens were numerically analysed subjected to a cyclic loading and constant axial load, analysing the model was done using the finite element analysis method by ANSYS software [16]. To validate the numerical analysis results, the analysed model was validated by comparing the results to previous experimental testing results conducted in a laboratory published by Aribert et al. [17]. The purpose of this paper is to improve the strength and performance of the composite column by investigating the effects of the cover concrete and

the steel-concrete coefficient of friction on fully encased composite columns subjected to cyclic load. Envelope curves analysis was conducted to analyse the cyclic behaviour of the composite encased columns investigated to determine their ductility and stiffness. In addition, the columns' ultimate axial load capacity, energy dissipation, ductility, and stiffness were investigated.

2. Research Methodology

This paper aims to improve the strength and the performance of the composite column. By investigating the cover concrete and the steel-concrete coefficient of friction on the behaviour (strength, ductility, stiffness, and energy dissipation) of composite columns under combined constant axial load and cyclically increasing load. The flowchart of the research methodology is shown in Figure 1.

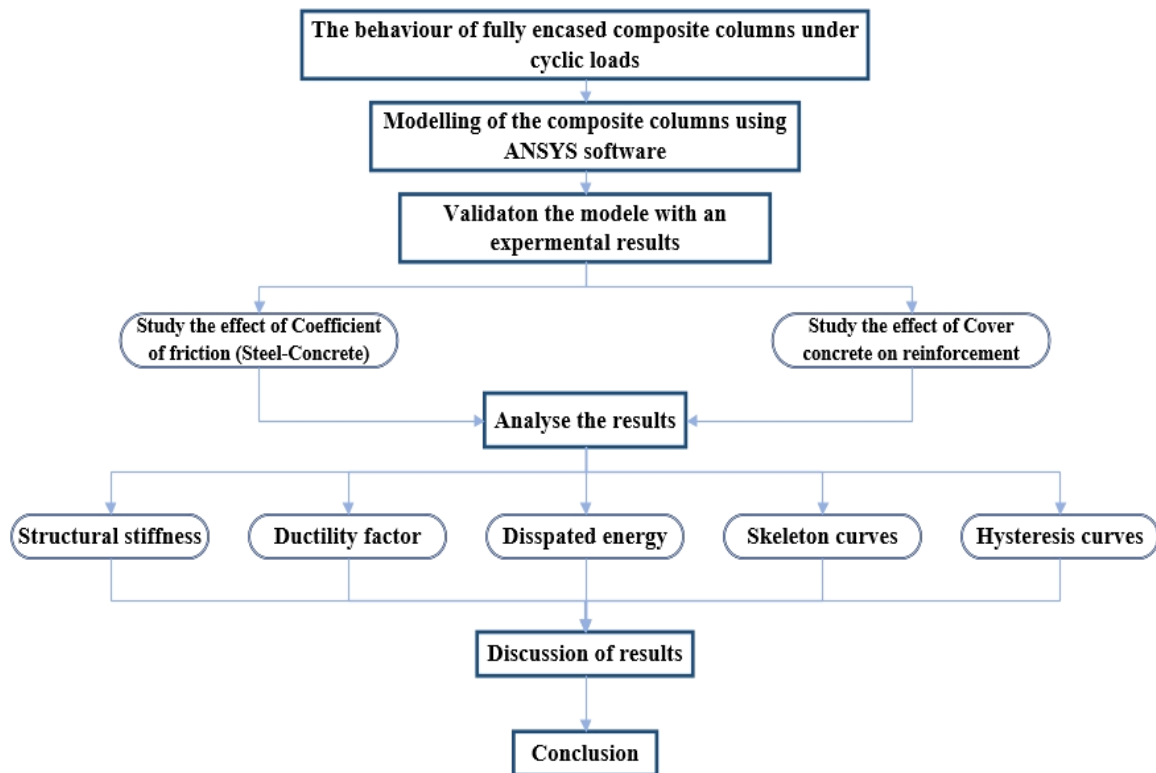


Figure 1. Flowchart of the research methodology

3. Finite Element Modelling

3.1. Geometrical and Material Properties

A two-series division of the composite columns' geometric dimensions was made. The first series (FEC.CC.1-FEC.CC.8) uses the same structural steel HEA240 (European H beam) section and reinforcing bars $4\phi 20$, but the cross-section is different. However, as indicated in Figure 2, the second series (FEC.CF.1-FEC.CF.11) has the same concrete cross-section 450×450 mm, structural steel HEA240 section, and reinforcing bars $4\phi 20$.

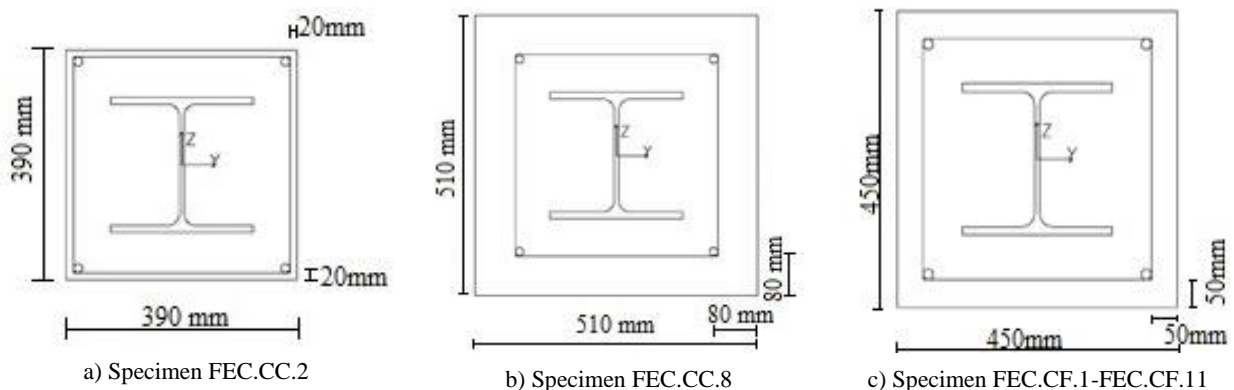


Figure 2. Dimensions of some designed composite columns

Steel has the properties of an elastoplastic material. To simplify the modelling of composite columns, a linear kinematic hardening model is utilized [18] to estimate the behaviour of steel under cyclic loads. In ANSYS, the characteristics of steel are specified as yield strength, modulus of elasticity, and Poisson's ratio among other things. According to Eurocode 3 [19], the modulus of elasticity is $E_s=210\,000$ MPa, the steel Poisson's ratio is 0.3, and the steel grades for structural steel sections and reinforcing bars are S275 ($f_y=275$ MPa) and S500 ($f_{sk}=500$ MPa), respectively, both classified as elastic perfectly plastic as shown in Figure 3:

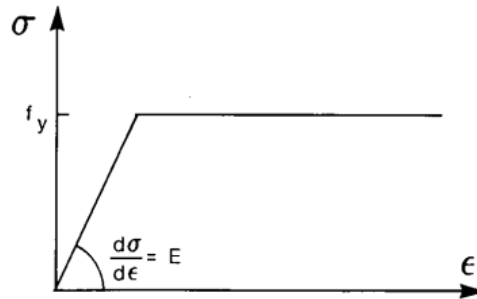


Figure 3. Steel material's stress-strain relationship [19]

The proposed model's concrete is an elastoplastic material. In Equation 1, The stress-strain relationship of concrete materials is used as illustrated in Figure 4, as recommended by Eurocode4 [20]. According to Eurocode2 [21], the Poisson's ratio of concrete (ν) is 0.2, and the modulus of elasticity is $E_{cm}=31000$ MPa.

$$\frac{\sigma_c}{f_{cm}} = \frac{k\eta - \eta^2}{1 + (K - 2)\eta} \tag{1}$$

where:

$$\eta = \epsilon_c / \epsilon_{c1}$$

$$K = 1,05 E_{cm} \times |\epsilon_{c1}| / f_{cm}$$

$\epsilon_{c1}=0.2\%$ is the strain at reaching the maximum strength.

$\epsilon_{cu1}=0.35\%$ is the ultimate strain.

$f_{cm}=33\text{MPa}$ is mean value of concrete cylinder compressive strength.

$f_t=1.2\text{MPa}$ is the value of the design tensile strength.

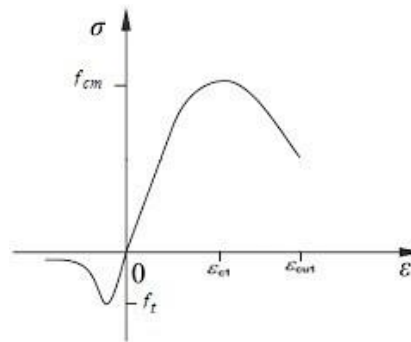


Figure 4. Concrete material's stress-strain relationship

3.2. General Configuration of the Composite Columns and Boundary Conditions

Considering several studies reported in the literature [12, 22-29], it was decided to choose the used finite element model Solid65, Solid185 and Link8 finite elements of the Ansys code [16]. The ANSYS code defined Solid65 as concrete in 3-D solid modelling with reinforcing bars for its ability to crack in tension and crush in compression. The element is made up of eight nodes, each with three degrees of freedom. The behaviour of this element with nonlinear material properties is the most important aspect of it. Concrete can crack, crush, and deform plastically. Rebar can resist tension and compression, as well as plastic deformation. The failure criterion for concrete due to multiaxial stress condition used in the study was the Willam- Warnke five parameter model [30], the failure surface could be defined by two constants, f_{cm} and f_t . Where f_{cm} is the ultimate uniaxial compressive strength and f_t is the concrete ultimate uniaxial tensile. To define concrete material, several properties must be entered into ANSYS, including the Poisson's ratio (ν), elastic modulus (E_{cm}), compressive uniaxial stress-strain relationship for concrete, ultimate uniaxial

compressive strength (f_{cm}), ultimate uniaxial tensile strength (f_t), and shear transfer coefficient, which represents the conditions of the crack plane. The shear transfer coefficient ranges from 0.0 to 1.0, with 0.0 representing a smooth crack (no shear transfer) and 1.0 indicating a rough crack (full shear transfer). The shear transfer for open cracks β_t and closed cracks β_c in this study is 0.75 and 0.9, respectively [28].

The structural steel section in a 3-D model is defined as Solid185 with eight nodes and three degrees of freedom at each node. Large deflection, plasticity, large strain capabilities, stress stiffening, and also creep are some of these element properties. The reinforcing bars are defined as Link8, which is a uniaxial compression-tension element with two nodes and three degrees of freedom at each node. [16]. Several finite element models with various element sizes were built to determine the most reasonable mesh that would provide accurate results while using the least amount of computing time to produce them with. The composite columns were found to work best with a mesh size of 30 mm. CONTA174 is used for the mesh of the concrete-steel interface to contact with the steel interface, and TARGE170 is used for the mesh of the concrete steel interface to contact with the concrete interface to simulate the interaction between steel and concrete [31-33]. Frictional contact is used between structural steel sections and concrete. Different friction coefficients ranging from 0.2 to 0.7 were used to investigate their influence on fully encased composite column behaviour in this paper. At the end of the column illustrated in Figure 5, the boundary conditions of the columns are clamped-free. After applying an axial force to the column's cross-sectional centroid, a horizontal load with displacement was applied using boundary conditions at different increment steps.

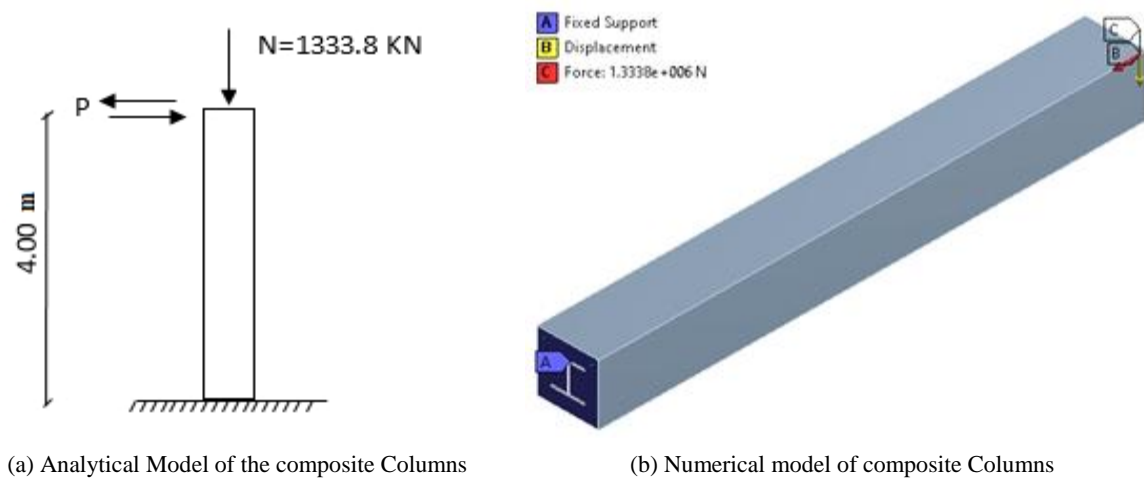


Figure 5. Boundary conditions of the composite column

According to Eurocode 4 [20], the columns were subjected to a prescribed horizontal displacement history under a constant axial load of $P=1333.8\text{kN}$, which was chosen as 20% of the plastic resistance of the composite cross-section to compressive axial force, $N_{pl,Rk}$, with $N_{pl,Rk} = A_a \cdot F_y + 0.85 A_c \cdot F_{ck} + A_s \cdot F_{sk}$. The effect of the applied axial load P is interesting to investigate subsequently. These loads were applied to the column's top surface. As seen in Figure 6, the horizontal displacement history is made up of a series of fully reversed displacement cycles.

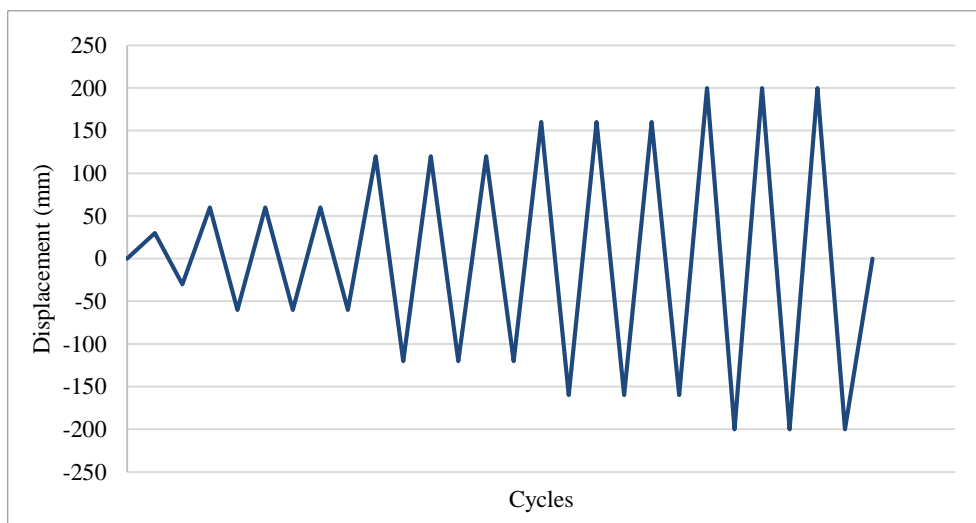


Figure 6. Cyclic applied horizontal displacement history

3.3. Validation of the Numerical Model

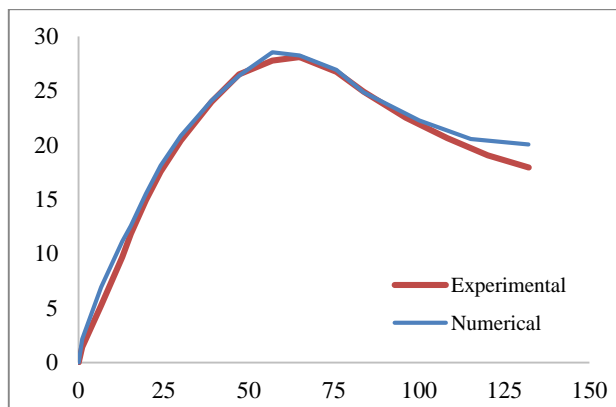
Four previously published test specimens by Aribert et al. [18] were used to evaluate the efficiency of the numerical model for the composite columns described in the preceding section. These four specimens can be classified according to the length of the column and type of loads. Table 1 lists the material parameters as well as geometrical properties. The experimental and numerical lateral displacement (v) versus lateral loads (P) curves are shown in Figure 7. As indicated in Table 2, the difference between numerical and experimental values for SI-1, S1-2, SIII-1, and SIII-2 specimens is +1.51, +0.66, -0.48, and +0.74 %, respectively. A comparison between the failure mode noted in the tests and those obtained by numerical simulation is illustrated in Figure 8. Overall, good agreement is established between the tested and numerical curves, as seen in Figure 7 (tested and numerical curves). This demonstrates that the current numerical model could be used to simulate the behaviour of fully encased composite columns under cyclic loading.

Table 1. The material parameters and the geometrical properties of the experimental test [17]

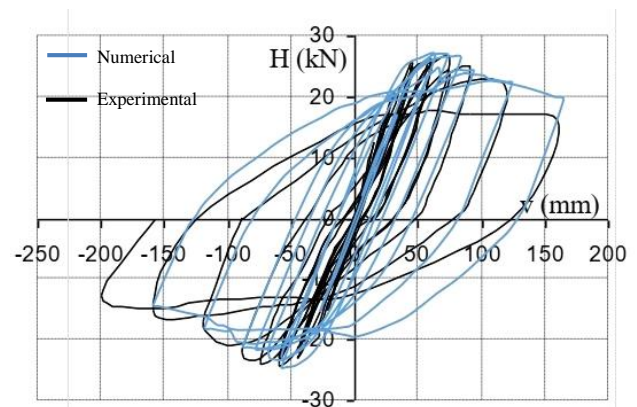
Specimen	Length (m)	Concrete class	f_{ck} (N/mm ²) (28 days on the cylinder)	E_{cm} (N/mm ²)	F_y (N/mm ²)	F_{sk} (N/mm ²)	E_a, E_{s2} (N/mm ²)
SI	2.00	C25	25.4	29000	302	560	20700
SIII	3.00	C25	24.5	29000	302	560	20700

Table 2. FEM lateral load values and experimental lateral load values

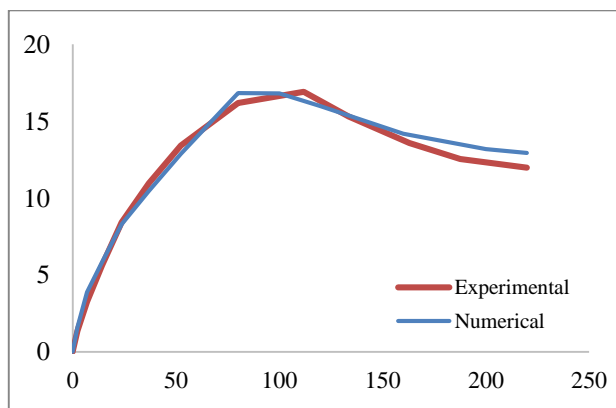
Specimen	Length (m)	Loads	P_{exp} (KN)	P_{FEM} (KN)	Difference (%)
SI-1	2.00	Monotonic	28.1	28.53	+1.51
SI-2	2.00	Cyclic	25.7	25.87	+0.66
SIII-1	3.00	Monotonic	16.9	16.82	-0.48
SIII-2	3.00	Cyclic	17.4	17.53	+0.74



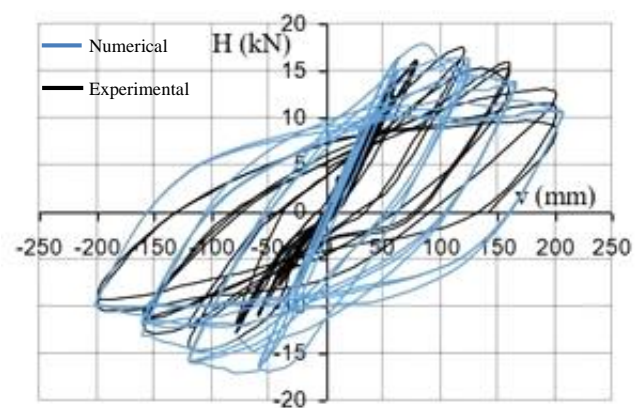
A) SI-1 Specimen



B) SI-2 Specimen



C) SIII-1 Specimen



D) SIII-2 Specimen

Figure 7. Numerical and experimental test lateral force-displacement curves comparison

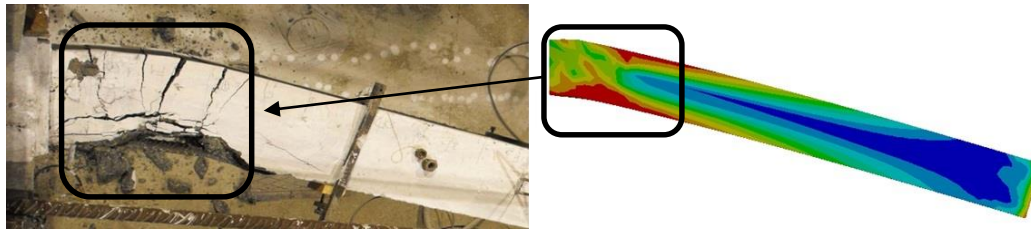


Figure 8. Comparison of typical failure mode of experimental and numerical specimen [3]

4. Results and Discussion

To understand the rigidity of this element before failure, the parameters of the cyclic response of the composite columns, as shown in Table 3, were investigated, including hysteresis curves, skeleton curves, ductility coefficient, dissipation energy, and initial stiffness. Figure 9 shows an example of the stress equivalent (Von-Mises) distribution of composite columns, it can be found that the columns reach the plastic mode at the bottom counter to the top of the columns still in the elastic mode. As illustrated in Figure 10, the deformed shape of the composite column at failure mode is also recorded. The finite element model predicted a steel yielding and concrete crushing as the failure mode. The compressive yield strength of concrete and yield stress of structural steel were both exceeded, respectively. The compressive stress was found to be highest near of the composite column bottom. The failure modes of the concrete and structural steel elements can be clearly identified by comparing the stresses of the elements to the strengths of the materials. Both modes of failure happen simultaneously, with the steel flange yielding initially accompanied by concrete crushing. The concrete fails in tension before the steel reaches its yield stress, while the concrete fails in compression before the concrete reinforcement reaches its yield stress. The next section contains further explanations and interpretations of the findings.

Table 3. Summary of the numerical results

specimens	Coeff.	c (mm)	Section	$N_{pl,Rk}$ (kN)	P_m (kN)	Δy (mm)	P_y (kN)	Δu (mm)	P_u (kN)	μ	E (kN.m)	K_y (kN/m)
FEC.CC.1		10	370×370	5459.24	136.37	68	122.5	200	131.77	2.94	341.81	1801.471
FEC.CC.2		20	390×390	5782.24	150.67	66	138.35	200	142.66	3.03	343.03	2096.212
FEC.CC.3		30	410×410	6122.24	171.34	65	154.42	200	137.92	3.08	379.91	2375.692
FEC.CC.4		40	430×430	6479.24	181.09	64.8	173.47	200	151.1	3.09	374.72	2677.006
FEC.CC.5		50	450×450	6853.24	198.65	64.2	194.28	200	164.34	3.12	378.45	3026.168
FEC.CC.6		60	470×470	7244.24	231.57	61.45	210.2	200	179.33	3.25	419.55	3420.667
FEC.CC.7		70	490×490	7652.24	237.11	60	218.43	200	193.52	3.33	421.64	3640.5
FEC.CC.8		80	510×510	8077.24	282.4	66	269.19	160	212.93	2.42	316.37	4078.636
FEC.CF.1	0.2			6853.24	160.37	48.5	148.78	80	165.58	1.65	37.54	3067.63
FEC.CF.2	0.25			6853.24	160.64	48.5	148.71	80	165.65	1.65	37.95	3066.19
FEC.CF.3	0.3			6853.24	161.57	62.5	171.93	150	107.4	2.40	163.34	2750.88
FEC.CF.4	0.35			6853.24	163.54	55.5	158.01	200	99.53	3.60	320.09	2847.03
FEC.CF.5	0.4			6853.24	165.49	55.5	163.97	200	87.23	3.60	327.08	2954.41
FEC.CF.6	0.45	-	450×450	6853.24	167.84	55.5	163.99	200	107.64	3.60	324.13	2954.77
FEC.CF.7	0.5			6853.24	169.45	55.5	164.01	200	99.69	3.60	321.5	2955.14
FEC.CF.8	0.55			6853.24	170.33	48.5	145.65	200	85.92	4.12	334.57	3003.09
FEC.CF.9	0.6			6853.24	172.84	48.5	148.65	200	86.55	4.12	347.26	3064.95
FEC.CF.10	0.65			6853.24	173.28	48.5	149.96	200	91.43	4.12	339.97	3091.96
FEC.CF.11	0.7			6853.24	176.27	48	153.51	200	100.75	4.17	331.75	3198.13

Coeff: the coefficient of the friction, c: the cover concrete, $N_{pl,Rk}$: characteristic value of the composite section's plastic resistance to compressive normal force, P_m : maximum lateral load that can be supported by the composite columns, μ : ductility factor, E: energy dissipation and K_y : stiffness initial.

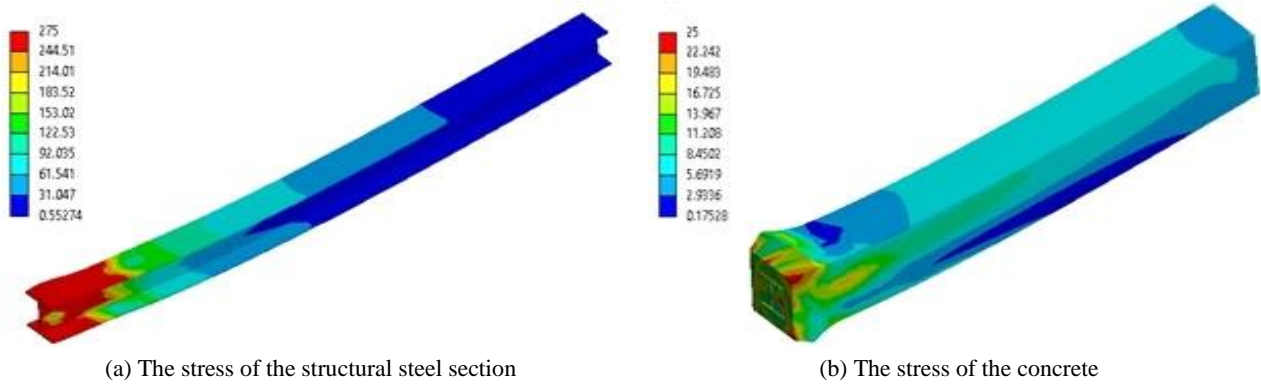


Figure 9. Von-Mises Stresses of composite column specimen FEC.CF.9 (steel and concrete)

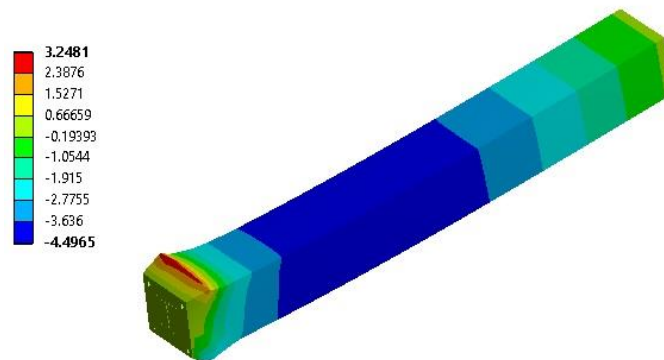
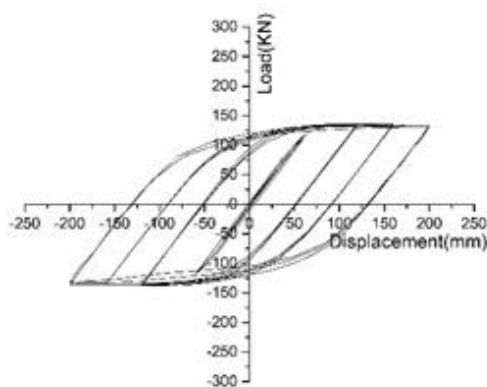


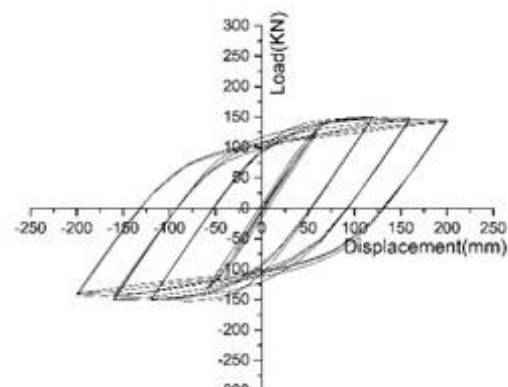
Figure 10. The deformed shape of composite column specimen FEC.CF.9

4.1. Hysteresis Curves

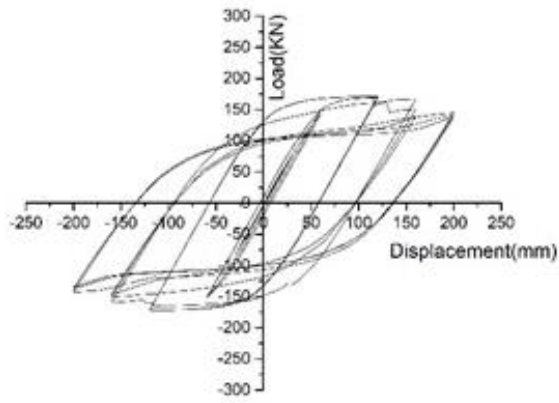
The load-lateral displacement curves of the structures contribute to a very important role to understand the inelastic behaviour in developing a seismic design methodology for these structures. As shown in Figure 10 the first series (FEC.CC.1-FEC.CC.8) among all the specimens, the test of specimen FEC.CC.8 failed to complete all the cycles, because the concrete cover is too high and the outer concrete is without reinforcement, all the hysteresis curves show high energy dissipation except the last one. It is observed that all specimens have some common hysteretic characteristics. The specimens have an elastic stage and a linear relationship between load and displacement at the early stages of loading, the hysteretic curves are symmetrical. After the cracking of the concrete, the specimens show an elastic-plastic response. As the lateral displacement increases, the hysteretic loops slowly approach the displacement axis. However, after the seventh cycle, the lateral load decreases under each displacement loading level, and loading and unloading gradually decrease stiffness for all specimens, due to spalling of the outer concrete and increasing loading displacement. On the other hand, the hysteresis curve gets plumper after the load reaches the ultimate load which explain a good energy dissipation capacity. All the specimens exhibit that has good cyclic behaviour except the last one. As shown in Figure 11, in the second series, the test of the specimen (FEC.CF.1-FEC.CF.3) failed to complete all the cycles because the coefficient of friction is too low, and the friction between structural steel and concrete prevent the ductility. All the hysteresis curves show high energy dissipation except the first three curves.



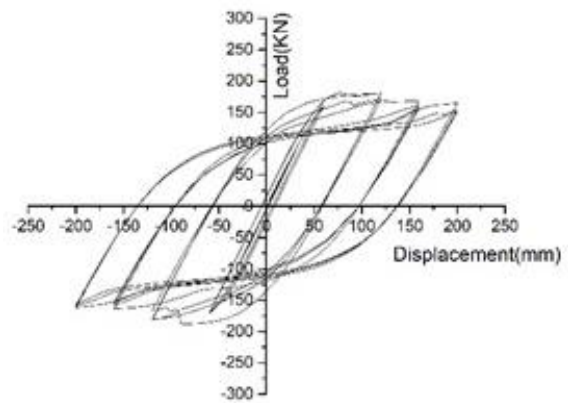
(a) FEC.CC.1



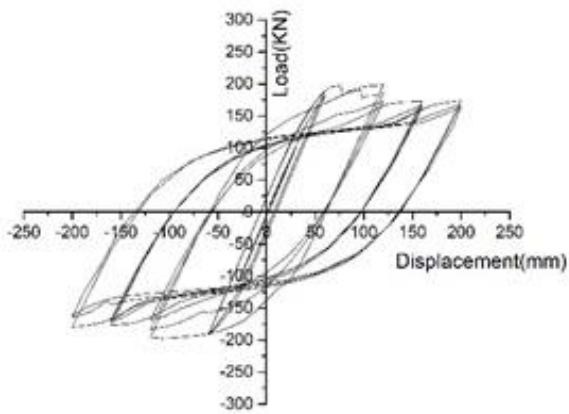
(b) FEC.CC.2



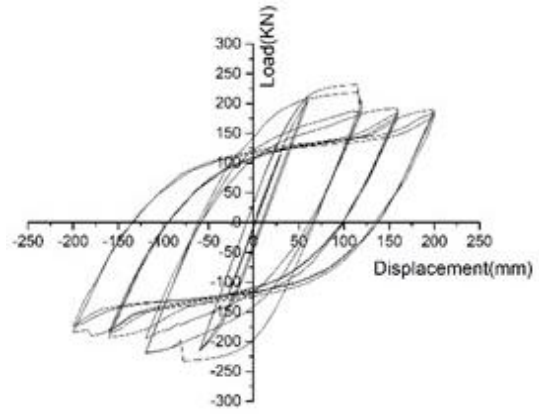
(c) FEC.CC.3



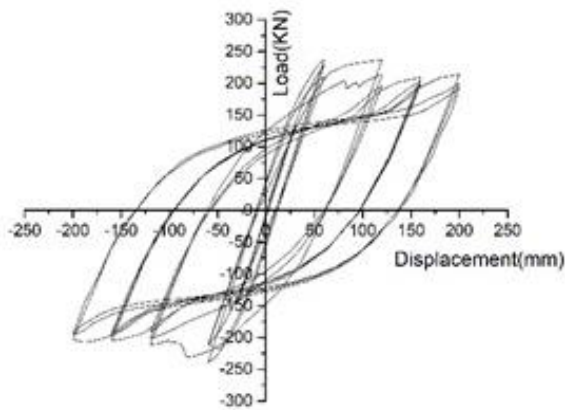
(d) FEC.CC.4



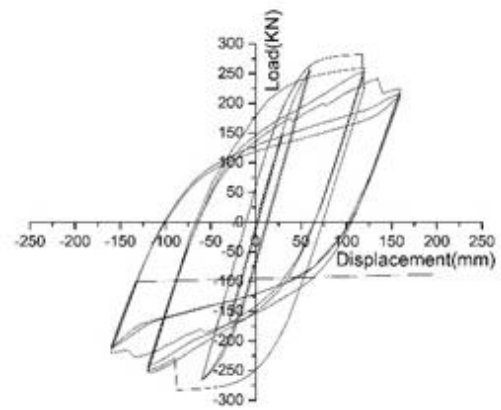
(e) FEC.CC.5



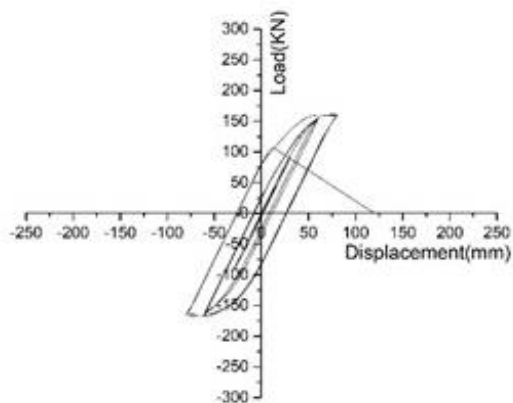
(f) FEC.CC.6



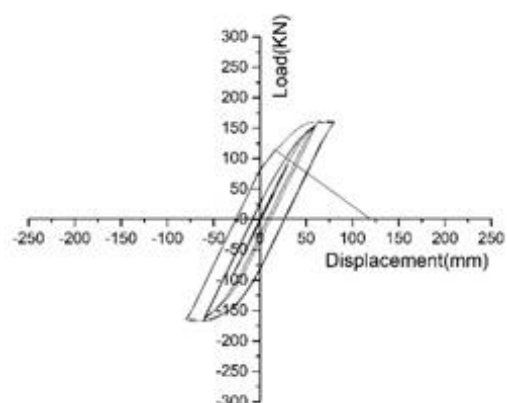
(g) FEC.CC.7



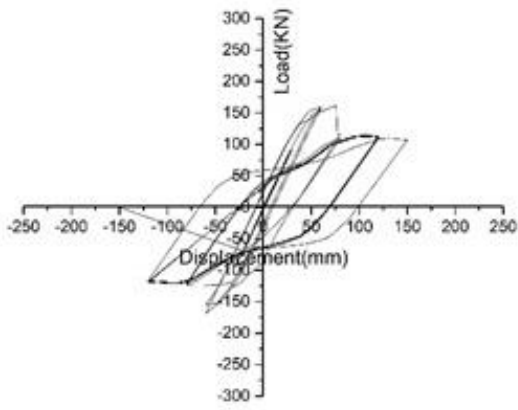
(h) FEC.CC.8



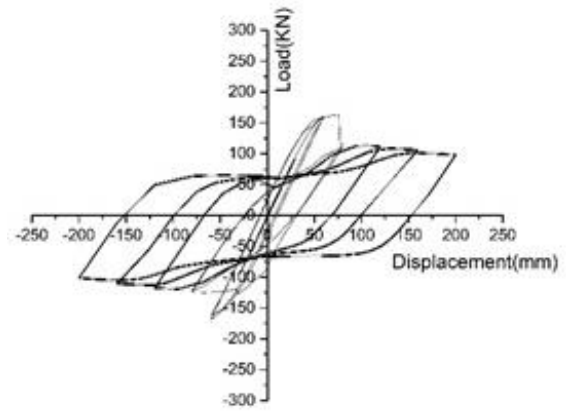
(i) FEC.CF.1



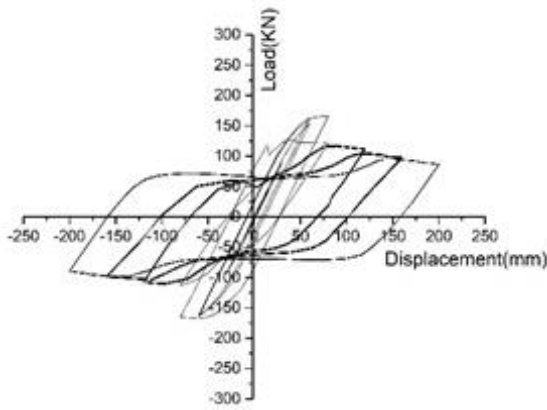
(j) FEC.CF.2



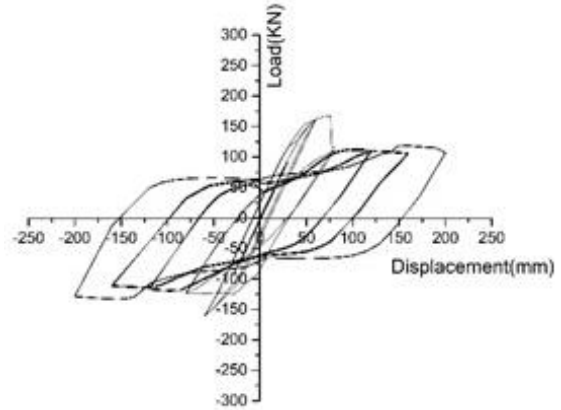
(k) FEC.CF.3



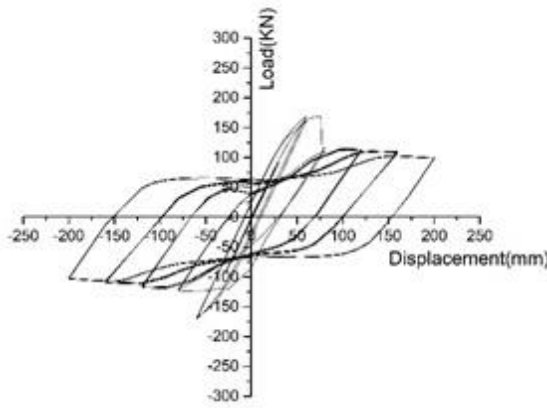
(l) FEC.CF.4



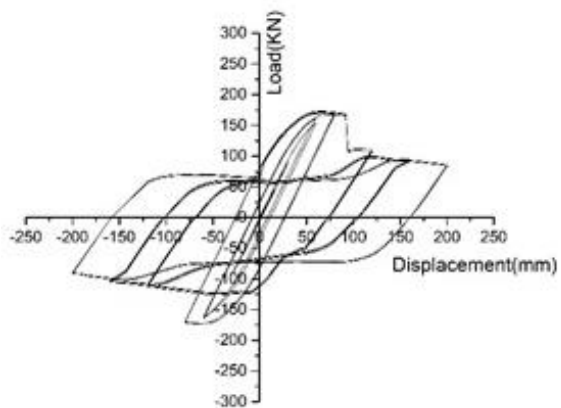
(m) FEC.CF.5



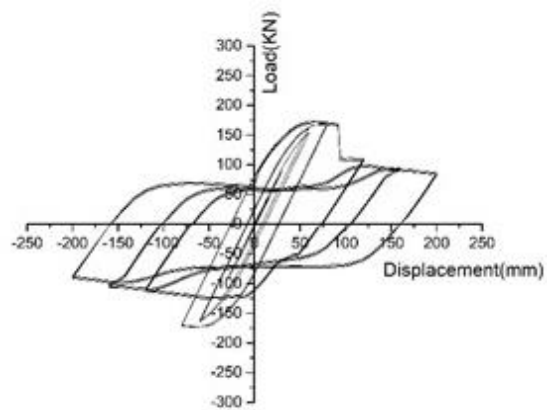
(n) FEC.CF.6



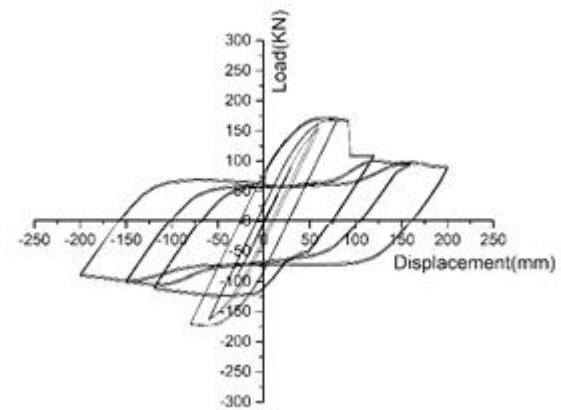
(o) FEC.CF.7



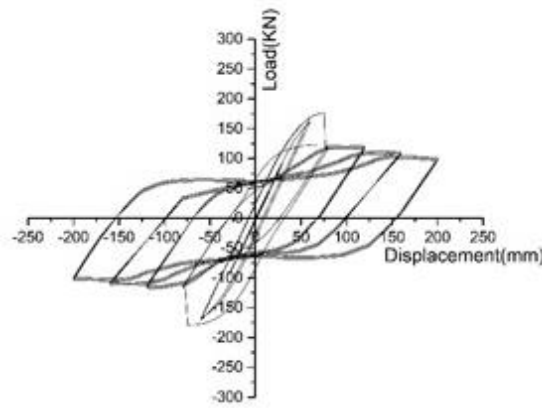
(p) FEC.CF.8



(q) FEC.CF.9



(r) FEC.CF.10



(s) FEC.CF.11

Figure 11. Hysteresis curves of the specimens (FEC.CC.1-FEC.CF.11)

4.2. Skeleton Curves

Skeleton curves were created by connecting the lateral load peak points and the corresponding horizontal displacement from each loading level's first cycle. An essential parameter is the skeleton curve, which measures ductility, strength, deformation capacity and the inelastic cyclic or seismic response of specimens, and is used for this purpose. The negative loading direction is determined in an analysis of the skeleton curve when the wider flange of inner structural steel is compressed, while the positive loading direction is established when the wider flange is tensioned [34]. The skeleton curves are shown in Figure 12 for easy comparison of the specimens. It is shown with increasing concrete cover the lateral load increases, the figure exhibit the discontinuity in the curves due to the spalling of the concrete cover [2].

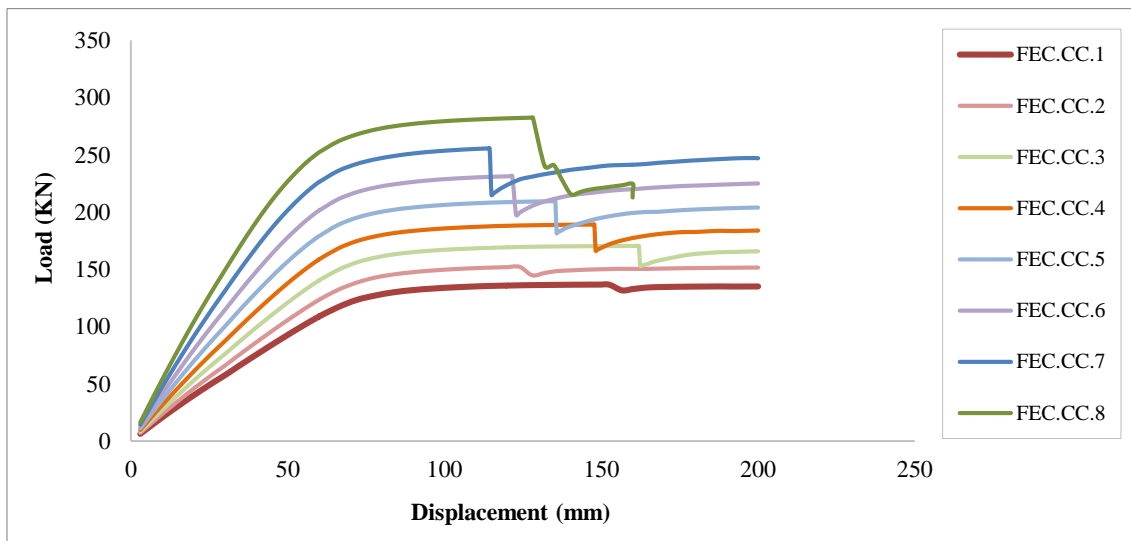


Figure 12. Comparison of skeleton curves

4.3. Dissipated Energy

The amount of energy dissipated by a structural element is an important factor in determining its seismic performance. The area contained by the hysteretic hoops is used to determine dissipated energy from the lateral load-displacement curve. In general, specimens with a lower concrete cover level had less dissipated energy than higher cover levels. The energy dissipation is shown in Table 3, with specimen FEC.CC.1 having a 341.81 kN.m dissipated energy according to the column's lower durability than the others, while FEC.CC.7 has a 421.64 kN.m dissipated energy, and specimen FEC.CC.8 reaching the failure mode at the end of the 10th cycle. However, with an increase of the concrete cover, the energy of a specimen tends to increase until it reaches 70 mm, it begins to decrease sharply, shown in Figure 13.a. The energy dissipation in the second series (FEC.CF.1-FEC.CF.11) at the beginning is low, and as the coefficient of friction increases also the energy increases until it reaches 0.6 then the energy degrades gradually. Figure 13.a indicates that the energy of the first specimen is 341.81 kN.m and the peak point is 421.64 kN.m. Figure 13.b shows that the energy of the first specimen, with 0.20 of friction coefficient is 37.54 kN.m and it increases and stabilized than the friction coefficient of 0.35. The peak point is 347.26 kN.m, which means that the coefficient of friction has an obvious effect over the cover concrete. But its effect is almost negligible from 0.35.

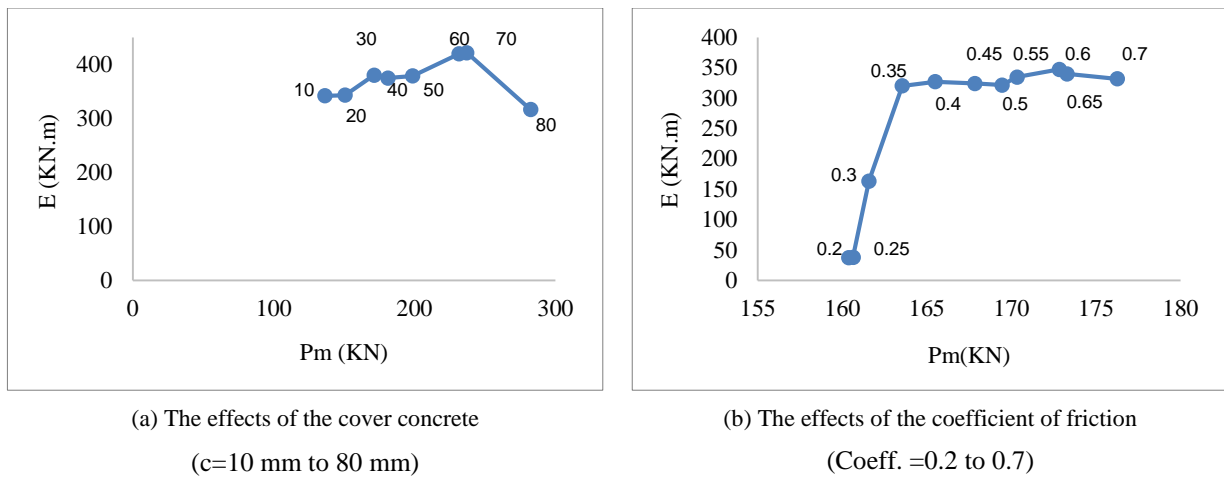


Figure 13. Cumulative energy and maximum lateral loads relationships

4.4. Ductility Factor

It is used to determine the cyclic or seismic behaviour of a structure's elements as well as their deformation capability. The ductility factor μ of a specimen is defined as the ratio of the ultimate displacement to the yield displacement $\mu = \Delta_u / \Delta_y$. Where, Δ_u is the ultimate displacement corresponding to ultimate load P_u and Δ_y is the yielding of the structural steel section displacement corresponding to yield load P_y .

For the first series (FEC.CC.1-FEC.CC.8), it is shown that the cover concrete thickness improves the ductility of the column. For a thick cover concrete, as 80 mm the column ductility decreases by 27.33%. Results in Table 3 indicate that FEC.CC.6 and FEC.CC.7 columns have better ductility than the others by +11.71% as shown in Figure 14.

For the second series (FEC.CF.1-FEC.CF.11) varying coefficient of steel-concrete friction, ductility generally increases proportionally. The first two columns have a low ductility, with the increase of the coefficient of friction the ductility increases, at specimen FEC.CF.4-FEC.CF.7 have constant ductility, but at specimen FEC.CF.8 it increases again, improving it by +12.62%.

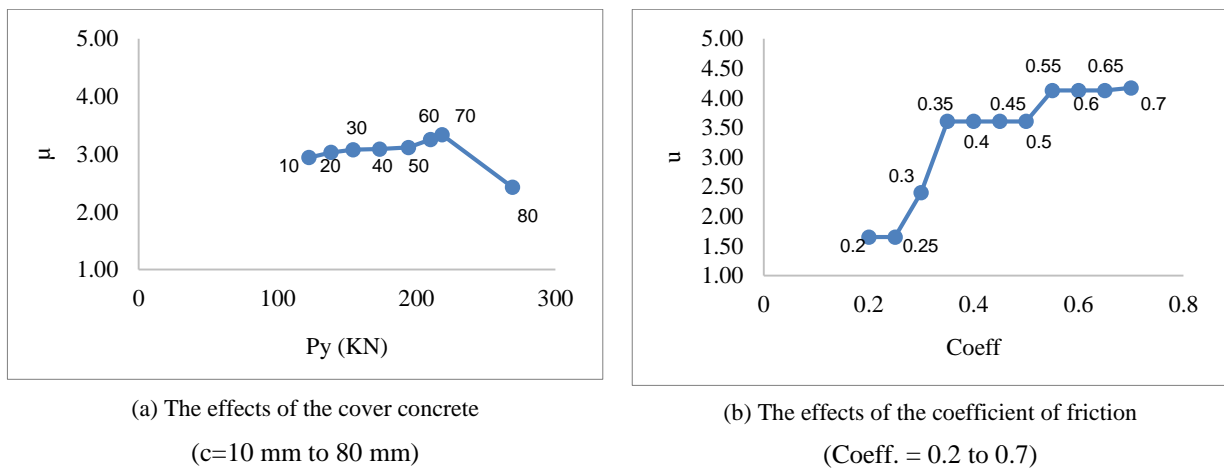


Figure 14. Ductility factor of the effects (cover concrete and coefficient of friction)

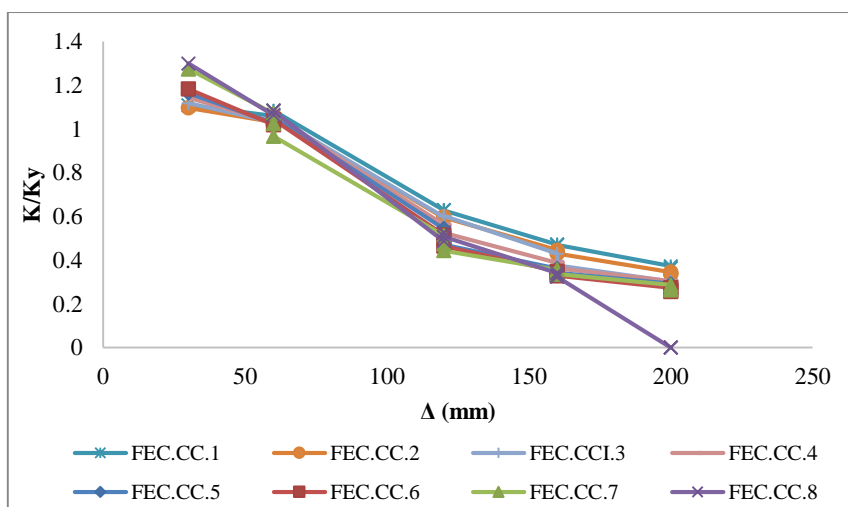
4.5. Structural Stiffness

Established by the numerical results, the main value of the rigidity of a column at the i^{th} drift has been evaluated by the Equation 2:

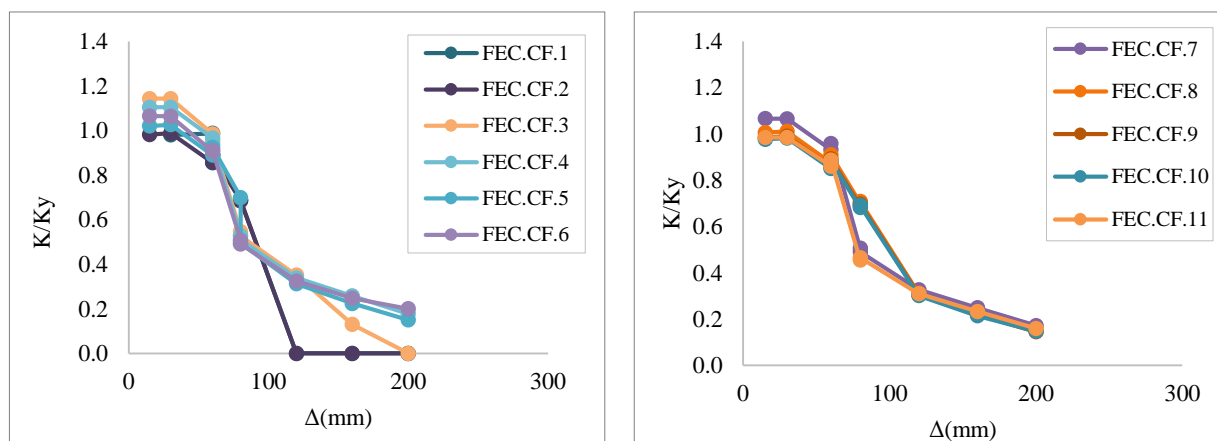
$$K_i = \frac{|+P_i| + |-P_i|}{|+\Delta_i| + |-\Delta_i|} \tag{2}$$

where $+\Delta_i$ and $-\Delta_i$ are the peak displacements of the cycle at the i^{th} lateral displacement level in two reversal directions respectively, $+P_i$ and $-P_i$ are the loads corresponding to the peak displacements respectively, [4]. Figure 15 describes the stiffness degradation curves of the specimens with the displacement, which K_y is the initial loop stiffness listed in Table 3. As exhibited in the curve, for the first series (FEC.CC.1-FEC.CC.8) the specimens with higher cover concrete

experienced stiffness degradation at an early stage of loading. This is mostly attributable to the restriction of the concrete crack. However, stiffness degradation is more obvious in the specimens with higher cover concrete. The stiffness gradually degrades as the lateral displacement increases, but it degrades significantly when the cover concrete thickness gets bigger. For the second series (FEC.CF.1-FEC.CF.11), with increases in the coefficient of friction, the stiffness at the 3rd cycle degrades seriously, until it reaches 0.6 then it degrades gradually.



(a) The effects of the cover concrete
(c=10 mm to 80 mm)



(b) The effects of the coefficient of friction
(Coeff. = 0.2 to 0.7)

Figure 15. The degradation of stiffness of the specimens

5. Conclusions

To understand the cyclic behaviour of composite columns, the effects of the cover concrete were numerically investigated, as well as the steel-concrete coefficient of friction by testing the columns under a combined cyclically increasing lateral load and constant axial load. Based on this study the following conclusions can be drawn:

- With an increase of the cover concrete, the displacement ductility, the energy dissipation and the stiffness increase by 11.71, 18.93 and 50.52% respectively compared with specimen FEC.CC.1. However, when the cover concrete is so large reaches 80 mm in the analysed specimens, the displacement ductility and the energy dissipation decrease by 27.33, 24.97% respectively, and the stiffness decreases seriously.
- After the load reaches the ultimate load, the hysteretic curves of the columns are plumped and affected by the spalling of cover concrete. Specimens (FEC.CC.1-FEC.CC.7) exhibit good ductility, energy dissipation capacity and good rigidity, counter to specimen FEC.CC.1.8 that failed to complete the test, it reached the failure mode at the end of the 10th cycle because the concrete cover is too high and the outer concrete is without reinforcement.
- With an increase of the coefficient of friction between steel and concrete, the ductility, the energy dissipation and the stiffness increase by 12.62, 7.82 and 7.11% respectively. However, when the coefficient of friction

reaches 0.6, it gives a better energy dissipation. It proves that the columns with a 0.6 coefficient of friction exhibit favourable cyclic behaviour.

- The coefficient of friction has an important effect on the cyclic behaviour of composite columns. The cyclic behaviour worsens when the coefficient of friction is decreased and it improves when the coefficient is increased, especially under 0.6.

The results show that the cover concrete has a slight impact on the composite columns, counter to the effects of the coefficient of friction owing that to the composite work between the steel section and the concrete. The sandblasting method of the steel in the composite column is necessary to improve the friction and to increase the dynamic dissipative capacity.

6. Declarations

6.1. Author Contributions

Conceptualization, A.A.; methodology, A.A. and N.B.; software, A.A. and N.B.; validation, A.A.; formal analysis, A.A.; investigation, A.A.; resources, A.A.; data curation, A.A.; writing—original draft preparation, A.A.; writing—review and editing, A.A., N.B. and K.H.; visualization, A.A.; supervision, N.B. and K.H.; project administration, A.A., N.B. and K.H. All authors have read and agreed to the published version of the manuscript.

6.2. Data Availability Statement

The data presented in this study are available in article.

6.3. Funding

The authors received no financial support for the research, authorship, and/or publication of this article.

6.4. Conflicts of Interest

The authors declare no conflict of interest.

7. References

- [1] Chen, C., Wang, C., & Sun, H. (2014). Experimental Study on Seismic Behavior of Full Encased Steel-Concrete Composite Columns. *Journal of Structural Engineering*, 140(6), 04014024. doi:10.1061/(asce)st.1943-541x.0000951.
- [2] Zhu, W., Jia, J., Gao, J., & Zhang, F. (2016). Experimental study on steel reinforced high-strength concrete columns under cyclic lateral force and constant axial load. *Engineering Structures*, 125, 191–204. doi:10.1016/j.engstruct.2016.07.018.
- [3] Campian, C., Nagy, Z., & Pop, M. (2015). Behavior of fully encased steel-concrete composite columns subjected to monotonic and cyclic loading. *Procedia Engineering*, 117(1), 439–451. doi:10.1016/j.proeng.2015.08.193.
- [4] Fang, L., Zhang, B., Jin, G. F., Li, K. W., & Wang, Z. L. (2015). Seismic behavior of concrete-encased steel cross-shaped columns. *Journal of Constructional Steel Research*, 109, 24–33. doi:10.1016/j.jcsr.2015.03.001.
- [5] Xu, C. H., Zeng, L., Zhou, Q., Tu, X., & Wu, Y. (2015). Cyclic performance of concrete-encased composite columns with T-shaped steel sections. *International Journal of Civil Engineering*, 13(4A), 456–467. doi:10.22068/IJCE.13.4.455.
- [6] Han, L. H., Liao, F. Y., Tao, Z., & Hong, Z. (2009). Performance of concrete filled steel tube reinforced concrete columns subjected to cyclic bending. *Journal of Constructional Steel Research*, 65(8–9), 1607–1616. doi:10.1016/j.jcsr.2009.03.013.
- [7] Gajalakshmi, P., & Helena, H. J. (2012). Behaviour of concrete-filled steel columns subjected to lateral cyclic loading. *Journal of Constructional Steel Research*, 75, 55–63. doi:10.1016/j.jcsr.2012.03.006.
- [8] Qian, W. W., Li, W., Han, L. H., & Zhao, X. L. (2016). Analytical behavior of concrete-encased CFST columns under cyclic lateral loading. *Journal of Constructional Steel Research*, 120, 206–220. doi:10.1016/j.jcsr.2015.12.018.
- [9] Shim, C. S., Chung, Y. S., & Han, J. H. (2008). Cyclic response of concrete-encased composite columns with low steel ratio. *Proceedings of the Institution of Civil Engineers: Structures and Buildings*, 161(2), 77–89. doi:10.1680/stbu.2008.161.2.77.
- [10] Hsu, H. L., Jan, F. J., & Juang, J. L. (2009). Performance of composite members subjected to axial load and bi-axial bending. *Journal of Constructional Steel Research*, 65(4), 869–878. doi:10.1016/j.jcsr.2008.04.006.
- [11] Ellobody, E., & Young, B. (2011). Numerical simulation of concrete encased steel composite columns. *Journal of Constructional Steel Research*, 67(2), 211–222. doi:10.1016/j.jcsr.2010.08.003.
- [12] Taufik, S., & Tjahjono, B. (2019). 3D ANSYS Modeling Behaviour of Encased Steel Composite Column with Wide Flange and Hollow Section. *International Journal of Mechanics and Applications*, 2019(1), 10–18. doi:10.5923/j.mechanics.20190901.02.

- [13] Chen, Y., Wang, T., Yang, J., & Zhao, X. (2010). Test and numerical simulation of partially encased composite columns subject to axial and cyclic horizontal loads. *International Journal of Steel Structures*, 10(4), 385–393. doi:10.1007/BF03215846.
- [14] Naito, H., Akiyama, M., & Suzuki, M. (2011). Ductility Evaluation of Concrete-Encased Steel Bridge Piers Subjected to Lateral Cyclic Loading. *Journal of Bridge Engineering*, 16(1), 72–81. doi:10.1061/(asce)be.1943-5592.0000120.
- [15] Yue, J., Qian, J., & Beskos, D. E. (2019). Seismic damage performance levels for concrete encased steel columns using acoustic emission tests and finite element analysis. *Engineering Structures*, 189(March), 471–483. doi:10.1016/j.engstruct.2019.03.077.
- [16] ANSYS, “APDL, Release 15.0.” (2013).
- [17] Aribert, J. M., Campian, C., & Pacurar, V. (2018). Monotonic and cyclic behaviour of fully encased composite columns and dissipative interpretation for seismic design. *Stessa 2003*, 115-121.
- [18] Chang, X., Wei, Y. Y., & Yun, Y. C. (2012). Analysis of steel-reinforced concrete-filled-steel tubular (SRCFST) columns under cyclic loading. *Construction and Building Materials*, 28(1), 88–95. doi:10.1016/j.conbuildmat.2011.08.033.
- [19] EN 1993-1-1/AC. (2009). Eurocode 3: Design of steel structures - Part 1-1: General rules and rules for buildings.
- [20] EN 1994-1-1/AC. (2004). Eurocode 4, Design of composite steel and concrete structures - Part 1-1: General rules and rules for buildings.
- [21] EN 1992-1-1/AC. (2004). Eurocode 2, Design of concrete structures - Part 1-1: General rules and rules for buildings.
- [22] Hussan, S. P., & Bashir, A. (2015). Analysis of Earthquake Resistant Properties of RC Core Steel Composite Columns & RCC Sections Using Finite Element Analysis. *International Journal of Engineering Trends and Technology*, 28(7), 359–364.
- [23] Si, B. J., Sun, Z. G., Ai, Q. H., Wang, D. S., & Wang, Q. X. (2008). Experiments and Simulation of Flexural-Shear Dominated Rc Bridge Piers Under Reversed Cyclic Loading. In *The 14th World Conference on Earthquake Engineering* (pp. 2–9).
- [24] Seres, N. (2008). Numerical modelling of shear connection between concrete slab and sheeting deck. In *7th fib international PhD symposium in civil engineering*. Stuttgart.
- [25] Alsamawi, A. bellah, & Boumechra, N. (2021). Behaviour of fully encased composite columns under cyclic loads. *Ce/papers*, 4(2-4), 564–569. doi:10.1002/cepa.1331.
- [26] Patil, P. S. S., Shaikh, A. N., & Niranjana, P. B. R. (2012). Non linear finite element method of analysis of reinforced concrete deep beam. *International Journal of Modern Engineering Research*, 2(6), 4622–4628.
- [27] Ibrahim, A. M., & Mahmood, M. S. (2009). Finite element modeling of reinforced concrete beams strengthened with FRP laminates. *European Journal of Scientific Research*, 30(4), 526–541.
- [28] Fauzan, Kurniawan, R., & Al Jauhari, Z. (2017). Finite element analysis of CES composite columns. *International Journal of Civil Engineering and Technology*, 8(10), 979–987.
- [29] Al Amli, A. S., Al-Ansari, N., & Laue, J. (2019). Study Numerical Simulation of Stress-Strain Behavior of Reinforced Concrete Bar in Soil using Theoretical Models. *Civil Engineering Journal*, 5(11), 2349–2358. doi:10.28991/cej-2019-03091416.
- [30] Fuschi, P., Dutko, M., Perić, D., & Owen, D. R. J. (1994). On numerical integration of the five-parameter model for concrete. *Computers and Structures*, 53(4), 825–838. doi:10.1016/0045-7949(94)90371-9.
- [31] Zhao, W. P. (2011). Local bond-slip numerical simulation based on ANSYS contact analysis. In *2011 International Conference on Electric Technology and Civil Engineering, ICETCE 2011 - Proceedings* (Vol. 0, pp. 438–441). doi:10.1109/ICETCE.2011.5775869.
- [32] Ibrahim, A., & Ahmed, Q. (2012). Finite element modeling of composite steel-concrete beams with external prestressing. *International Journal of Civil & Structural Engineering*, 3(1), 101–116.
- [33] De Nardin, S., Almeida Filho, F. M., Oliveira Filho, J., Haach, V. G., & El Debs, A. L. H. C. (2005). Non-linear analysis of the bond strength behavior on the steel-concrete interface by numerical models and pull-out tests. *Proceedings of the Structures Congress and Exposition*, 1077–1088. doi:10.1061/40753(171)107.
- [34] Xu, C. H., Zeng, L., Zhou, Q., Tu, X., & Wu, Y. (2015). Cyclic performance of concrete-encased composite columns with T-shaped steel sections. In *International Journal of Civil Engineering* (Vol. 13, Issue 4A, pp. 456–467). doi:10.22068/IJCE.13.4.455.